ELSEVIER

Tectonophysics 286 (1998) 31–46

TECTONOPHYSICS

The San Gabriel Mountains bright reflective zone: possible evidence of young mid-crustal thrust faulting in southern California

Trond Ryberg [a,*], Gary S. Fuis [b]

[a] *GeoForschungsZentrum, Telegrafenberg, 14473 Potsdam, Germany*
[b] *U.S. Geological Survey, 345 Middlefield Road - MS 977, Menlo Park, CA 94025, USA*

Abstract

During the Los Angeles Region Seismic Experiment (LARSE), a reflection/refraction survey was conducted along a line extending northeastward from Seal Beach, California, to the Mojave Desert, crossing the Los Angeles basin and San Gabriel Mountains. Shots and receivers were spaced most densely through the San Gabriel Mountains for the purpose of obtaining a combined reflection and refraction image of the crust in that area. A stack of common-midpoint (CMP) data reveals a bright reflective zone, 1-s thick, that dominates the stack and extends throughout most of the mid-crust of the San Gabriel Mountains. The top of this zone ranges in depth from 6 s (~18-km depth) in the southern San Gabriel Mountains to 7.5 s (~23-km depth) in the northern San Gabriel Mountains. The zone bends downward beneath the surface traces of the San Gabriel and San Andreas faults. It is brightest between these two faults, where it is given the name San Gabriel Mountains 'bright spot' (SGMBS), and becomes more poorly defined south of the San Gabriel fault and north of the San Andreas fault. The polarity of the seismic signal at the top of this zone is clearly negative, and our analysis suggests it represents a negative velocity step. The magnitude of the velocity step is approximately 1.7 km/s. In at least one location, an event with positive polarity can be observed 0.2 s beneath the top of this zone, indicating a thickness of the order of 500 m for the low-velocity zone at this location. Several factors combine to make the preferred interpretation of this bright reflective zone a young fault zone, possibly a 'master' decollement. (1) It represents a significant velocity reduction. If the rocks in this zone contain fluids, such a reduction could be caused by a differential change in fluid pressure between the caprock and the rocks in the SGMBS; near-lithostatic fluid pressure is required in the SGMBS. Such differential changes are believed to occur in the neighborhood of active fault zones, where 'fault-valve' action has been postulated. Less likely alternative explanations for this velocity reduction include the presence of magma and a change in composition to serpentinite or metagraywacke. (2) It occurs at or near the brittle–ductile transition, at least in the southern San Gabriel Mountains, a possible zone of concentrated shear. (3) A thin reflection rising from its top in the southern San Gabriel Mountains projects to the hypocenter of the 1987 *M* 5.9 Whittier Narrows earthquake, a blind thrust-fault earthquake with one focal plane subparallel to the reflection. Alternatively, one could argue that the bends or disruptions in the reflective zone seen at the San Gabriel and San Andreas faults are actually offsets and that the reflective zone is therefore an older feature, possibly an older fault zone.

Keywords: crustal structure; bright spot; San Andreas Fault Zone; brittle-ductile; transition; low-velocity zone; reflection seismics

* Corresponding author. Fax: +49 (331) 8877-520; E-mail: trond@gfz-potsdam.de

0040-1951/98/$19.00
PII S0040-1951(97)00253-9

1. Introduction

The Los Angeles Region Seismic Experiment (LARSE) was initiated by the U.S. Geological Survey and the Southern California Earthquake Center in an attempt to better define crustal structure to seismogenic depths in the Los Angeles region. This survey was motivated by the recent occurrence of moderate earthquakes on previously unknown faults in the Los Angeles basin, including the 1971 *M* 6.5 San Fernando, 1987 *M* 5.9 Whittier Narrows, and 1994 *M* 6.7 Northridge earthquakes. An important goal of LARSE was to image faults, especially blind thrust faults (Fuis et al., 1996).

LARSE began in 1993 with a passive experiment along a profile from Seal Beach to the Mojave Desert, crossing the Los Angeles basin and San Gabriel Mountains (Kohler and Davis, 1997), and was followed in 1994 by active experiments along three lines criss-crossing the Los Angeles region, including a line coincident with the passive experiment (Line 1, Fig. 1; Fuis et al., 1996). Most of the data acquired in 1994 were designed to obtain a combined reflection and refraction image of the San Gabriel Mountains and the San Gabriel Valley, a basin peripheral to and just north of the Los Angeles basin (Fig. 1). Preliminary results from 1994 include a velocity model along Line 1, obtained by inversion of first arrivals, and a reflection image of the San Gabriel Mountains and San Gabriel Valley (Fuis et al., 1996). The reflection image contains a bright reflective zone in the mid-crust, beginning at 6- to 7.5-s two-way traveltime. This reflective zone is approximately coextensive with the San Gabriel Mountains, although it is brightest between the San Andreas and San Gabriel faults, where it is given the name San Gabriel Mountains 'bright spot' (SGMBS). It is approximately 1-s thick and contains reflection amplitudes that are, on average in unprocessed seismograms, at least 9 dB above background (Fig. 2).

In its depth and brightness, the reflective zone resembles other seismic-reflection 'bright spots' reported from around the world. These include bright spots at Socorro, New Mexico (Sanford et al., 1977; Brown et al., 1980), Death Valley, California (de Voogd et al., 1986), Snake Range, Nevada (Hauser et al., 1987), Black Forest, Germany (Lueschen et al., 1987), Surrency, Georgia (Pratt et al., 1991), Buena Vista Valley, Nevada (Jarchow et al., 1993), and Tibet (Makovsky et al., 1996). Amplitude–decay curves for several of these bright spots were compared in Jarchow et al. (1993) and are reproduced here along with a similar curve for the San Gabriel Mountains (Fig. 2). In all of these curves, the bright spots have amplitudes 7–15 dB above background. The Socorro, Death Valley, Black Forest, and Tibetan bright spots have been attributed to the presence of fluid — possibly magma — in the mid-crust; the Surrency bright spot, to a solid–solid reflective interface. The bright spot in Buena Vista Valley, Nevada, has been interpreted as evidence for magma at the base of the crust. We report here evidence that the San Gabriel Mountains bright reflective zone is, at least in its upper part, a strong low-velocity zone that most likely contains fluids. The configuration of the top of this zone, which dips or steps upward to the south, toward the hypocenter of the Whittier Narrows earthquake, is suggestive of a blind thrust fault, possibly a master decollement. The San Gabriel Mountains bright zone is the only one in the above list to occur in a transpressive regime; most of the bright spots occur in extensional regimes.

2. Geologic setting

Southern California is a geologically complex region. Line 1 was chosen to minimize 3-D structure; it traverses three markedly different regions, including the Los Angeles and San Gabriel Valley basins, the central Transverse Ranges (San Gabriel Mountains), and the Mojave Desert (Fig. 1).

The Los Angeles basin occupies a region at the juncture of three geologic provinces (Wright, 1991). It lies at the eastern end of the (offshore) Continental Borderland, south of the Transverse Ranges, and at the northwestern end of the Peninsular Ranges (Fig. 1). The present-day Los Angeles basin began its evolution in Late Miocene time by subsidence between the right-oblique Whittier and Palos Verde fault zones and the left-oblique Santa Monica/Raymond fault system (Wright, 1991). The San Gabriel Valley, a peripheral basin, began its evolution by subsidence between the Whittier fault and a hingeline located at the Chino fault (Wright, 1991). Beginning in mid-Pliocene time and continuing today, deformation of both the Los Angeles and San

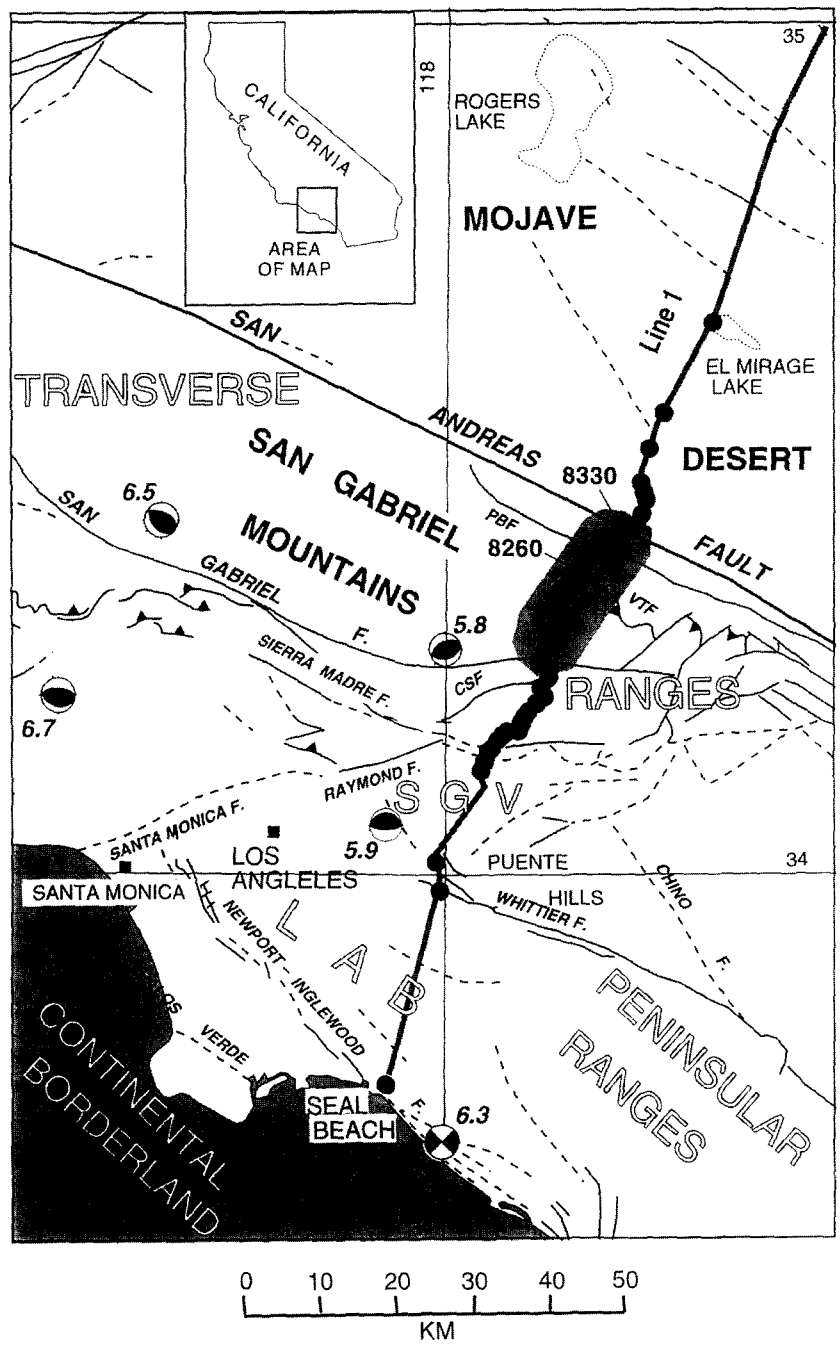

Fig. 1. Fault map of Los Angeles region, southern California, showing explosive sources (black dots) and receivers (gray line) along LARSE Line 1 and moderate earthquakes from the last 70 years (shown with focal mechanisms and magnitudes). '8260' and '8330' are shotpoint locations referred to in the following figures. *CSF* = Clamshell–Sawpit fault; *LAB* = Los Angeles basin; *PBF* = Punchbowl fault; *SGV* = San Gabriel Valley; *VTF* = Vincent thrust fault. Gray patch, region of brightest part of reflective zone (San Gabriel Mountains bright spot, SGMBS). Focal mechanisms were obtained as follows: 1933 *M* 6.3 Long Beach (Hauksson, 1987); 1971 *M* 6.5 San Fernando earthquake (Whitcomb, 1971); 1987 *M* 5.9 Whittier Narrows earthquake (Hauksson et al., 1988); 1991 *M* 5.8 Sierra Madre earthquake (Hauksson, 1994); and 1994 *M* 6.7 Northridge earthquake (Hauksson et al., 1995).

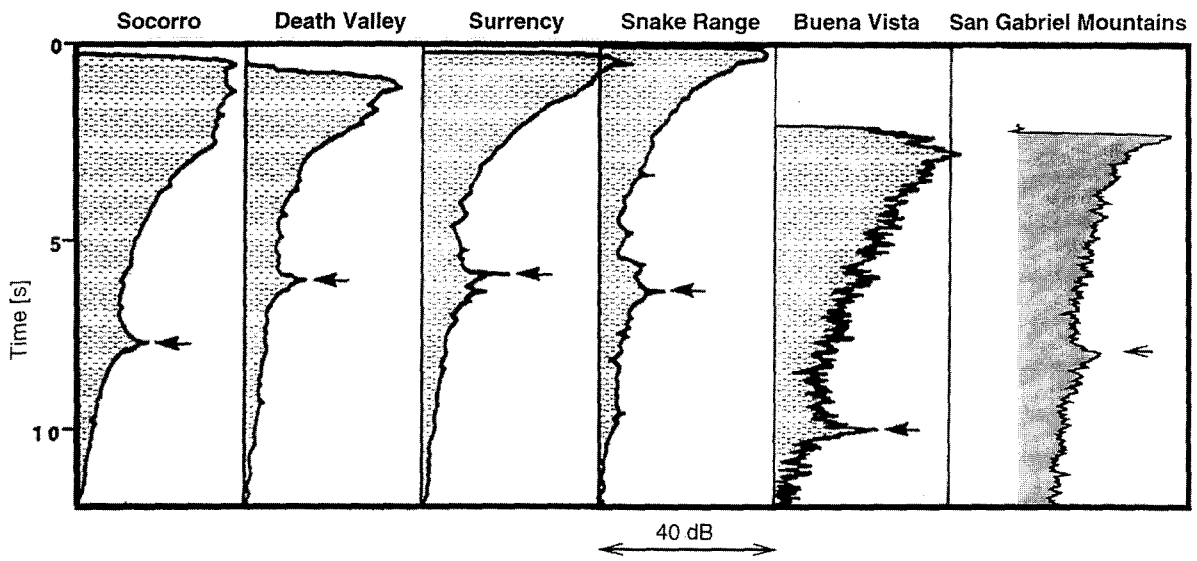

Fig. 2. Amplitude–decay curves for SGMBS compared to other bright spots (adapted from Jarchow et al., 1993). Like amplitudes of other bright spots, amplitudes of SGMBS are well above background (9 dB maximum).

Gabriel Valley basins has involved southward shortening of the crust and the propagation of blind thrust faults beneath the basins. The 1987 *M* 5.9 Whittier Narrows earthquake occurred on one of these blind thrust faults (Hauksson et al., 1988), and the 1991 *M* 5.8 Sierra Madre earthquake occurred on a branch of the Sierra Madre fault system (Clamshell–Sawpit fault (CSF), Fig. 1; Hauksson, 1994). For examples of balanced cross-sections along and near Line 1, see Davis and Namson (1989), Wright (1991), and Shaw and Suppe (1996).

The Transverse Ranges are late Cenozoic, east–west-trending ranges that have resulted from compression across the left-stepping bend in the San Andreas fault and from block rotations. In the central Transverse Ranges, or San Gabriel Mountains, Mesozoic plutonic rocks and Precambrian gneissic rocks form the chief upper-plate rocks. The Vincent thrust fault separates these upper-plate rocks from the lower-plate Pelona Schist, a near-shore, late Mesozoic sedimentary sequence that was metamorphosed during subduction in the latest Mesozoic or earliest Cenozoic (Fig. 1; Ehlig, 1981). Much of the San Gabriel Mountains — indeed much of southern California — may be underlain at depth by the Pelona Schist (Ehlig, 1981). The rocks of the San Gabriel Mountains are offset by several older branches of the San Andreas fault system, including the San Gabriel and Punchbowl faults (Fig. 1; Ehlig, 1981; Powell, 1993). They are juxtaposed against sedimentary rocks of the San Gabriel Valley basin along the Sierra Madre reverse fault system and against rocks of the Mojave Desert along the San Andreas fault. In addition to reverse faulting along the Sierra Madre fault system, north–south shortening is being accommodated by broad arching across the interior and northern margin of the range (Ehlig, 1981).

The San Gabriel Mountains have not experienced the substantial (near 90°) rotations observed in the western Transverse Ranges (west of Fig. 1; see Hornafius et al., 1986), which are interpreted to have occurred on mid- to lower-crustal decollements (Nicholson et al., 1994). Powell (1993) has modeled chiefly translational motions of the component blocks of the San Gabriel Mountains along various branches of the San Andreas fault.

3. Data acquisition

LARSE included detonation of 62 explosions, from 10 to 2000 kg, along Line 1 (Fig. 1). These explosions were recorded by a stationary, linear array of 640 seismographs. Shots and receivers were spaced most densely through the northern San

Gabriel Valley and San Gabriel Mountains: 1000-m spacing for shots and 100-m spacing for receivers. Source–receiver offsets ranged from 0 to 160 km. Approximately one half of the receivers in the dense interval were 3-component. The reader is referred to Murphy et al. (1996) for details of the acquisition.

4. Data processing

4.1. Shape of the bright zone

Most of the shot gathers in the central part of Line 1 are dominated by a strong reflection at approximately 6 to 7.5 s two-way traveltime (Fig. 3; Fig. 4, features A and B). The reflection is strongest in shot gathers between the San Gabriel and San Andreas faults. The reflections occur over a time interval of as much as 1 s. This interval exceeds the normal pulse length of the first arrival, which ranges from 0.2 to 0.5 s (Figs. 3 and 4), and thus indicates either structure within the reflective zone or multiples.

In order to examine the shape of the reflective zone, it was necessary to bring it into better focus than in Fuis et al. (1996). To accomplish this, processing was done in several stages:

(1) The traveltime effects of velocity variations in the upper 5 km, taken from Fuis et al. (1996) and from W.J. Lutter (written commun., 1995), were re-

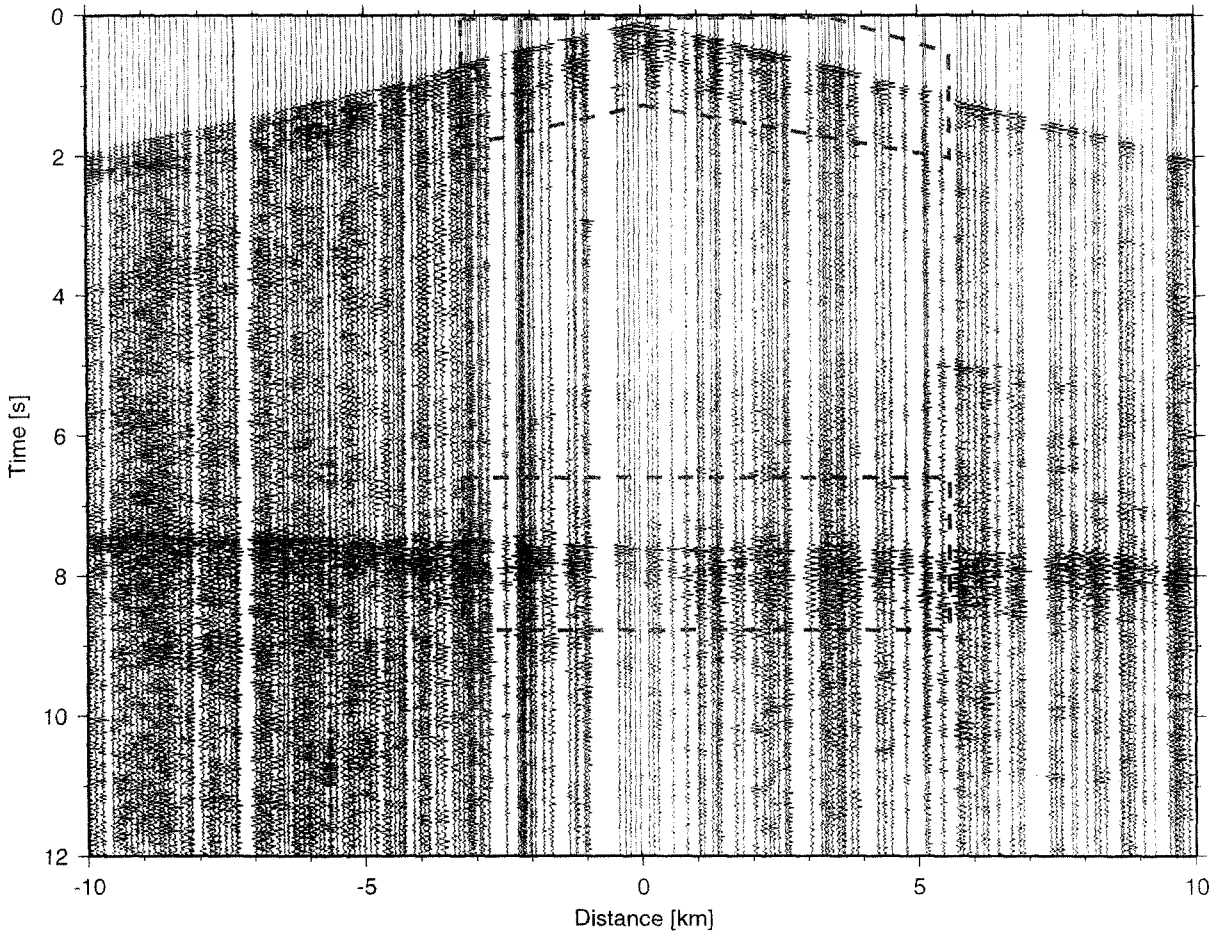

Fig. 3. Shot gather for shotpoint (SP) 8260 (see Fig. 1 for location). Boxes indicate portions of seismic traces used in Fig. 5A. These data are vertical-component and have been bandpass-filtered (8–12–40–50 Hz), corrected for spherical divergence, and trace normalized. Note: no AGC has been applied. A strong band of reflectivity (SGMBS) dominates section at 7–8 s.

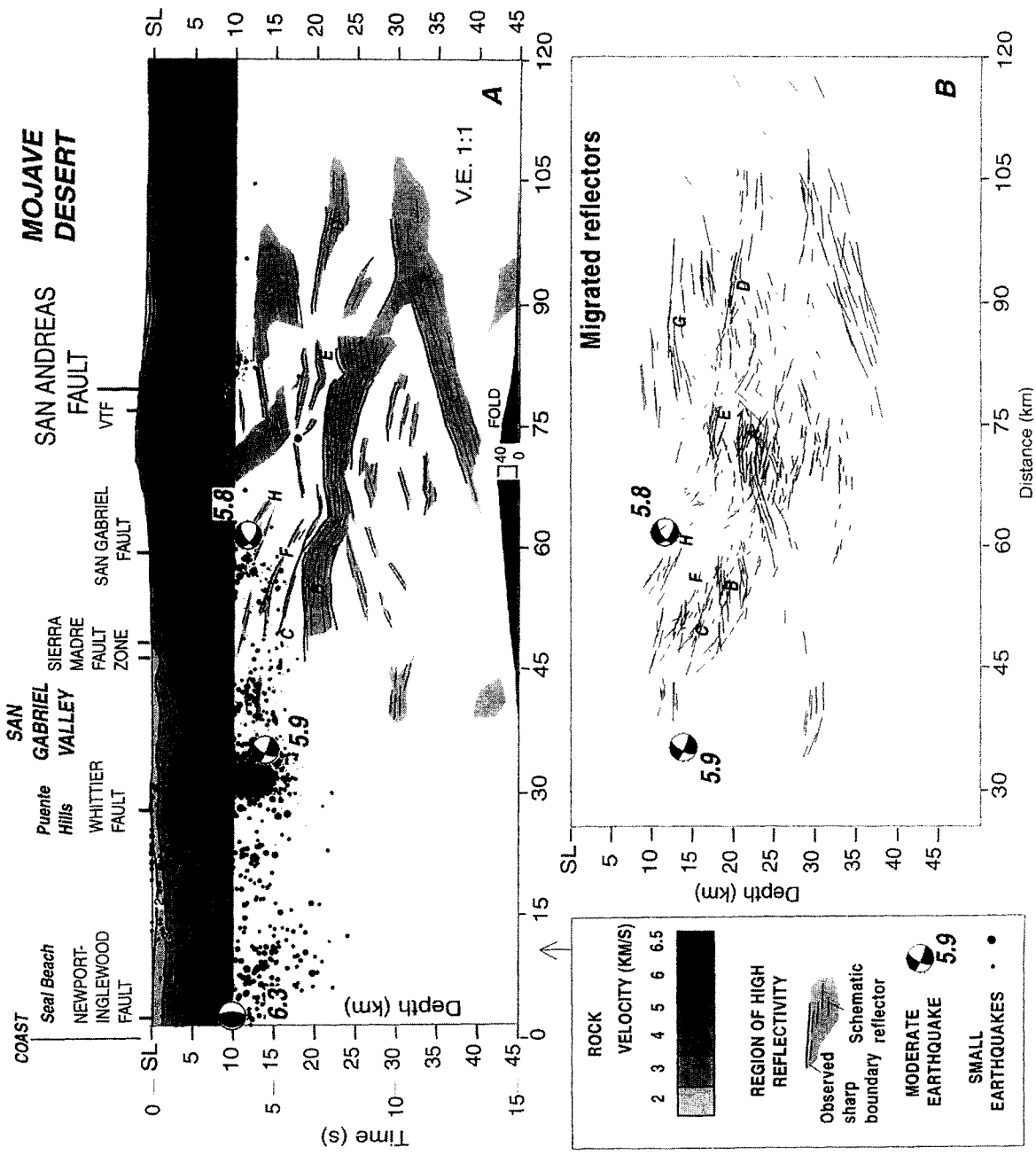
LOS ANGELES BASIN
SAN GABRIEL MTS
MOJAVE DESERT
COAST
Seal Beach
NEWPORT-INGLEWOOD FAULT
Puente Hills
WHITTIER FAULT
SAN GABRIEL VALLEY
SIERRA MADRE FAULT ZONE
SAN GABRIEL FAULT
SAN ANDREAS FAULT
VTF
SL
Time (s)
Depth (km)
6.3
5.9
5.8
V.E. 1:1
A
FOLD
Migrated reflectors
B
Distance (km)
ROCK VELOCITY (KM/S)
2 3 4 5 6 6.5
REGION OF HIGH REFLECTIVITY
Observed sharp boundary
Schematic reflector
MODERATE EARTHQUAKE
SMALL EARTHQUAKES

moved; vertical-incidence traveltimes through this region were replaced with traveltimes through a 5-km/s medium.

(2) Topographic variations were removed; sources and receivers were placed at sea level.

(3) Envelopes were calculated for each seismic trace, normalized, corrected for normal moveout, binned, and stacked to produce a common mid-point (CMP) image of the San Gabriel Mountains and northern San Gabriel Valley (T. Ryberg, G.S. Fuis, W.J. Lutter, and others, in preparation). Envelopes were stacked rather than actual seismic traces, because reflections were still not coherent enough after the above steps to produce a useful image.

(4) In order to perform a migration of the data, a line drawing was made of the CMP image (Fig. 4A). In making this line drawing, we found it useful to add schematic reflectors within and subparallel to the boundaries of reflective zones, with densities appropriate to convey the strength of each zone.

(5) Finally, the line drawing was migrated with a constant velocity of 6.0 km/s to obtain an improved image of reflector geometry (Fig. 4B).

Features appear more continuous in the unmigrated than in the migrated image. The bright reflective zone (features A and B, Fig. 4A) extends throughout most of the mid-crust of the San Gabriel Mountains. The top of this zone ranges in depth from 6 s (~18-km depth) in the southern San Gabriel Mountains to 7.5 s (~23-km depth) in the northern San Gabriel Mountains. The zone bends downward beneath the surface traces of the San Gabriel and San Andreas faults — sharply so at the San Andreas fault. It is brightest between these two faults, and becomes more poorly defined south of the San Gabriel fault and north of the San Andreas fault. Unfortunately, north of the San Andreas fault, CMP fold is much reduced, and a clear image of the zone, if it exists, was not obtained. Perhaps importantly, there are thin reflections above the bright reflective zone — within about 1 s of its top — that roughly mimic its shape. One such reflection rises from the top of the zone south of the San Gabriel fault (feature C, Fig. 4A). Other such reflections exhibit a downward kink at the San Andreas fault (feature E, Fig. 4A). The downward kinks in reflective zones A and E at the San Andreas fault may represent either unmodeled delays in the fault zone below 5-km depth (see processing step 1 above) or may represent real disruption of these reflectors by the fault zone.

In the migrated image, the bright reflective zone breaks up into two compact, or 'spot'-like, features (A and B, Fig. 4B). Feature A is referred to as the San Gabriel Mountains 'bright spot' (SGMBS). Unfortunately, any continuity or disruption of the bright reflective zone through the vicinity of the San Gabriel or San Andreas fault is lost in this image. In contrast, features D and E appear to move toward each other in this image, suggesting continuity of this reflective zone above the SGMBS (across the deep projection of the San Andreas fault).

4.2. Polarity and fine structure of the bright zone

To analyze the polarity of the reflection at the top of the bright spot, a direct comparison with first arrivals was made using raw data from two of the best shot gathers, SP 8260 and SP 8330 (see Fig. 1 for locations). Because the complexities of velocity structure and topography above the bright zone could not be completely removed (see processing steps 1 and 2 above), the bright-zone reflections do not align perfectly along a sharp hyperbola (Fig. 3). To sharpen the reflection onset, the dominant trough in the first part of the band was picked, and these picks were used to produce time-aligned sections, where first arrivals and reflections could be compared directly (panels 2 and 3, respectively, Fig. 5A,B). The first arrivals are characterized by a positive (red) onset, as expected from explosions, and the reflections,

Fig. 4. (A) Combined velocity model and line drawing of CMP data along LARSE Line 1. Moderate earthquakes that are near Line 1 (see Fig. 1) are projected onto image, as well as earthquakes from the Southern California Seismic Network catalog from the last 20 years within zone 40 km wide (small black dots of various size). See text for discussion of labeled features A–H. (B) Line-drawing migration of reflectors shown in (A). Constant velocity of 6 km/s was used for migration. Note. Sierra Madre earthquake is interpreted to have occurred on Clamshell–Sawpit fault (CSF, Fig. 1; Hauksson, 1994), which terminates at about Line 1. We projected this earthquake onto our cross-section parallel to east–west-trending structures of the main Sierra Madre fault zone. If we had projected this earthquake onto our cross-section parallel to strike of CSF, it would be approximately 10 km north of position shown.

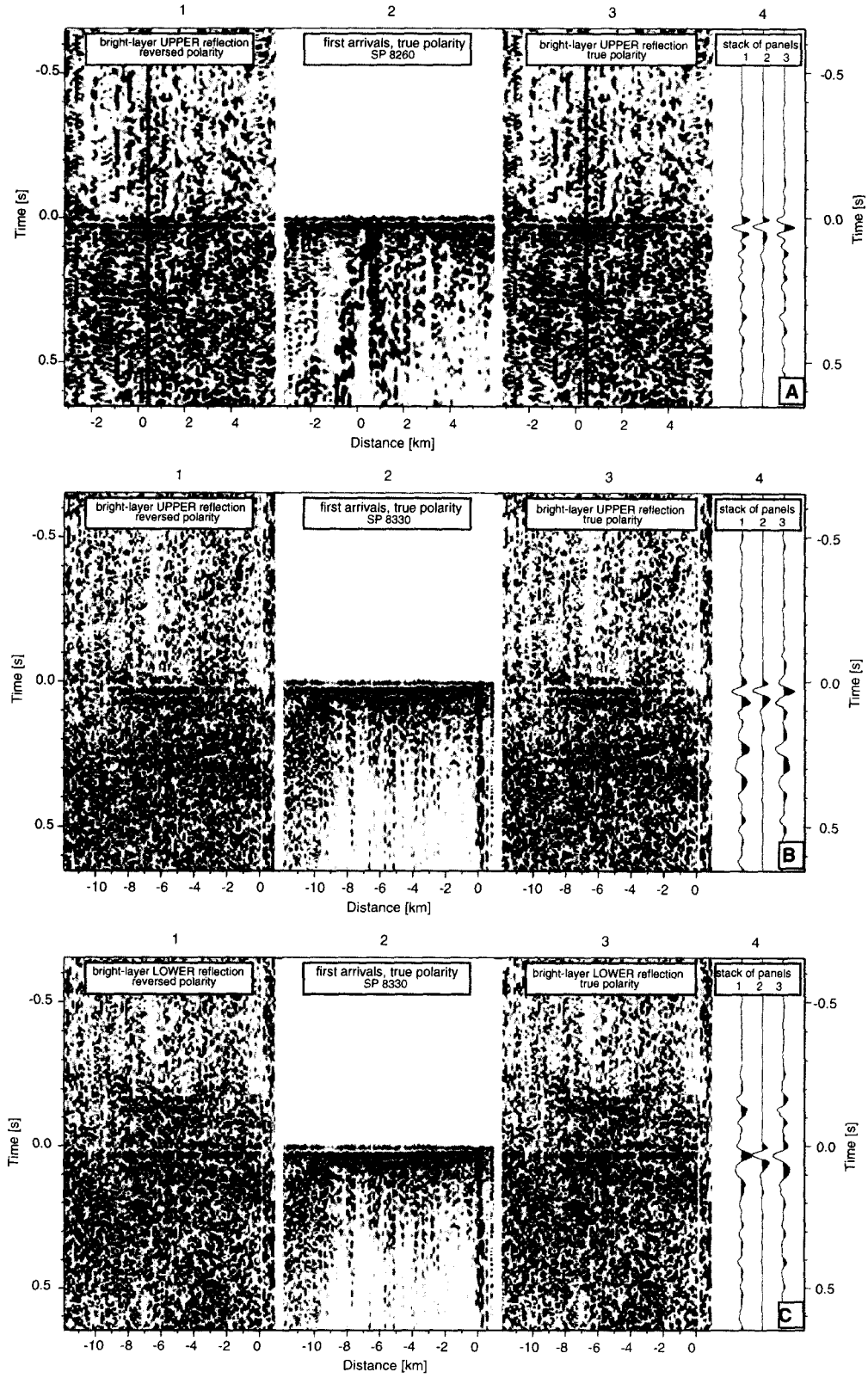
1
2
3
4
bright-layer UPPER reflection reversed polarity
first arrivals, true polarity SP 8260
bright-layer UPPER reflection true polarity
stack of panels 1 2 3
Time [s]
-0.5
0.0
0.5
-2 0 2 4
Distance [km]
A
bright-layer UPPER reflection reversed polarity
first arrivals, true polarity SP 8330
bright-layer UPPER reflection true polarity
stack of panels 1 2 3
-10 -8 -6 -4 -2 0
Distance [km]
B
bright-layer LOWER reflection reversed polarity
first arrivals, true polarity SP 8330
bright-layer LOWER reflection true polarity
stack of panels 1 2 3
-10 -8 -6 -4 -2 0
Distance [km]
C

by a negative (blue) onset. Stacking of these time-aligned arrivals (panels 4, Fig. 5A,B) demonstrates that the first arrivals and reflections have a similar waveform but reversed from each other. This fact suggests that a simple negative velocity step is responsible for the reflection rather than, for example, constructive interference caused by 'tuning' from a thin layer (~1/4 wavelength thick). Reflection from a thin layer would produce some distortion of the source wavelet which should be visible, given the low noise level produced by the stacking of traces (panels 4, Fig. 5A,B). Another important observation, especially from SP 8330, is appearance of a second strong reflection following the first by about 0.2 s (Fig. 5B). Aligning the traces of this second reflector (Fig. 5C), a procedure requiring additional shifts (caused by background noise) of generally less than 10 ms, reveals a positive reflection polarity and, again, a waveform similar to that of the first arrival, but in this case, the frequency content appears to be slightly shifted toward lower frequencies. Comparing the amplitudes of both reflections we find that the average estimated impedance contrast of the lower boundary is ~5% higher than that of the upper one, a fact that suggests that the second reflection is not a multiple of the first. Thus, we infer that the top and the bottom of a low-velocity zone in the uppermost part of the bright zone consists of subequal velocity steps, opposite in sense, separated by about 0.2 s. Given the slightly lower frequency content of the second reflection, we cannot rule out the possibility of a steep velocity gradient instead of a step.

Other information to constrain the polarity of the bright spot can be obtained by studying wide-angle and horizontal-component data. The existence and position of a critical P-wave reflection and the existence of converted phases can be used to evaluate whether the impedance contrast is positive or negative. We constructed a super CMP gather (Fig. 6), i.e. we selected all traces with source–receiver midpoints between 72- and 77-km model distance (within the SGMBS). The super CMP gather for the vertical component shows clearly the direct P and S waves and the PP reflection from the bright spot. At distances greater than 20 km, the PP reflection disappears, indicating that there is most likely no critical point and no postcritical PP reflection. In Fig. 6C, we show expected PP amplitude behavior, based on Zoeppritz equations (Aki and Richards, 1980), for both positive and negative velocity steps. We conclude that the PP amplitudes are most consistent with a negative velocity step. For both the vertical component and the combined horizontal components (Fig. 6A and Fig. 6B, respectively), the super CMP gather shows a phase at a traveltime (11 s) appropriate for a P–S (or S–P) conversion. On the horizontal components, this 11-s phase peaks in amplitude between about 10 and 20 km, approximately consistent with expected amplitude behavior for P–S (or S–P) conversions for either a positive or negative velocity step (Fig. 6C). Both Fig. 6A and Fig. 6B also show a diffuse phase between 13 and 15 s interpreted as Moho or near-Moho reflectivity.

4.3. Amplitude of the bright-zone reflection

To model the impedance contrast required to produce the uppermost SGMBS reflection, we calculated synthetic seismograms using the reflectivity method (Fuchs and Mueller, 1971) and a velocity model averaged for the central San Gabriel Mountains (Fig. 4A, Fig. 7F) containing low-velocity

Fig. 5. (A) Panel 2 shows data from Fig. 3, upper box, that have been aligned using first-arrival picks. Traces are normalized, and amplitudes are represented by colors; red for positive amplitudes and blue for negative amplitudes. No other processing was applied to data (no filtering, no spherical divergence or AGC corrections). Panel 3 shows data from Fig. 3, lower box, that have been aligned using first-trough picks of uppermost bright-spot reflection; this reflection is referred to as 'upper reflection'. Data are displayed as in panel 2. Panel 1 gives the same data as panel 3, but polarity has been reversed for easier comparison with first arrivals of panel 2. Panel 4 contains three seismograms: the first is stack of data in panel 1; the second is stack of data in panel 2; and the third is stack of data in panel 3. These stacked seismograms reveal that bright-spot reflection has waveform similar to first arrival but polarity is clearly reversed. (B) Similar display as in (A) but for SP 8330 (see Fig. 1 for location). One reaches same conclusion: bright-spot reflection has same waveform as first arrival but polarity is clearly reversed. (C) Repetition of (B) but trace alignment in panels 1 and 3 is achieved using first-peak picks for reflection that is seen 0.2 s below top of bright reflective zone in (B); this reflection is referred to as 'lower reflection'. Here, one concludes that this reflection has similar waveform *and* polarity as first arrival.

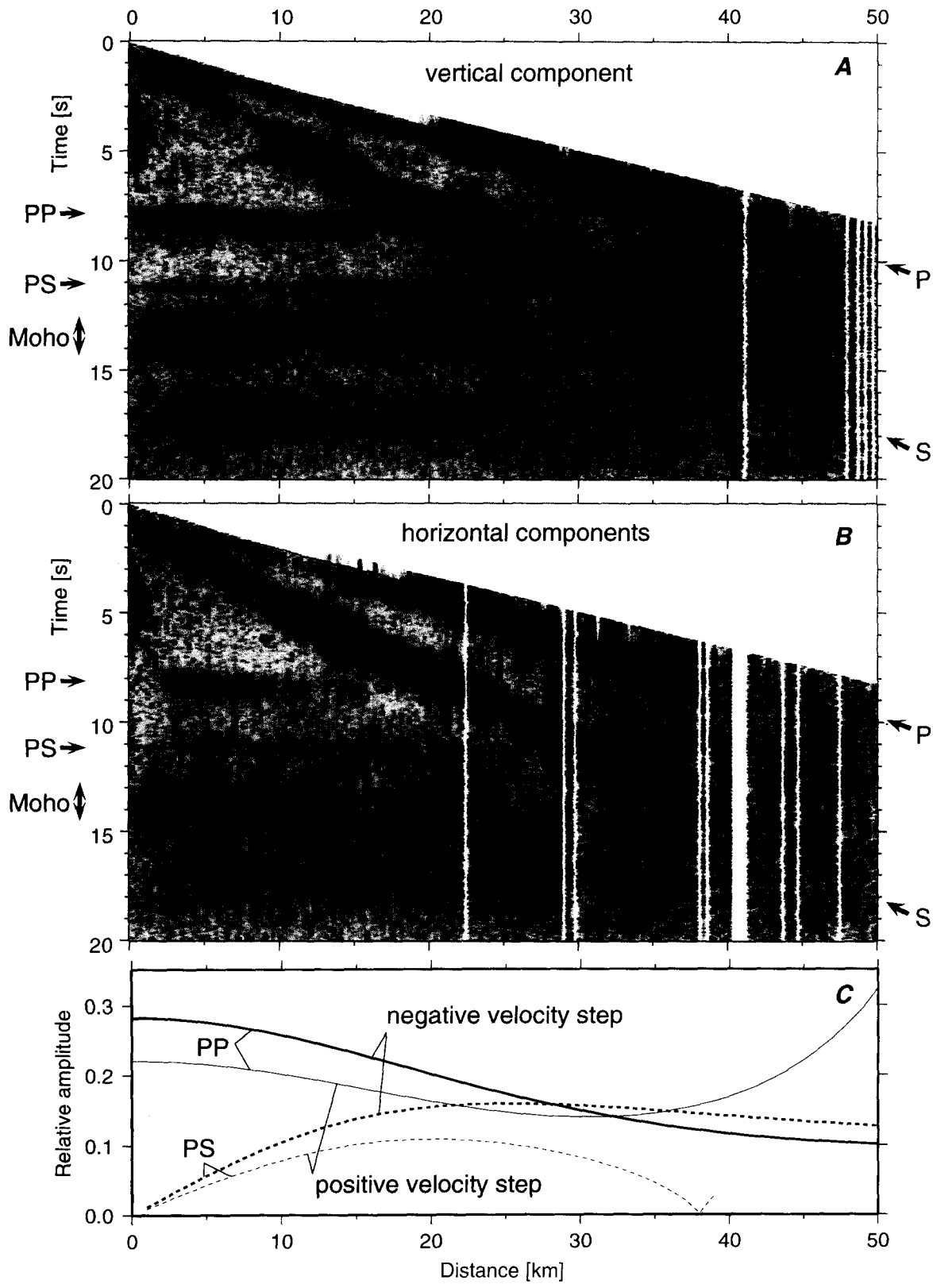
A
vertical component
Time [s]
PP
PS
Moho
P
S
B
horizontal components
Time [s]
PP
PS
Moho
P
S
C
negative velocity step
PP
PS
positive velocity step
Relative amplitude
Distance [km]

zones of various strengths. In this model, the S-wave velocity was chosen to be $V_p/\sqrt{3}$, and the density was chosen to be correlated to V_p according to Birch (1961). We used a realistic Q structure, with attenuation ranging from 6 to 27 in the upper 300 m (Fletcher et al., 1990; Aster and Shearer, 1991) in order to produce synthetic first arrivals similar to those observed (Fig. 7A). Comparison of relative reflection strength between observed and synthetic data, using either diagrams in which the velocity reduction in the low-velocity zone is varied in discreet increments for the synthetic data (Fig. 7B–E) or a diagram in which a curve is interpolated through such velocity reductions (Fig. 7G), one concludes that a velocity reduction near 1.5 km/s (1.7 ± 0.3 km/s from Fig. 7G) best matches the observed data (Fig. 7A). This result appears surprisingly robust. We used a different velocity model of the upper 5 km (dashed curve, Fig. 7F), generated from matching averaged first-arrival traveltimes in the central San Gabriel Mountains to 20-km offset (using an infinite Q), and also concluded that the best-fitting velocity reduction was about 1.5 km/s.

5. Discussion: preliminary tectonic interpretation

In the southern San Gabriel Mountains, earthquakes projected onto the CMP section (from 20 km on either side) terminate in depth at about the top of the bright reflective zone, or at least near a thin reflector that diverges upward from this zone south of the San Gabriel fault (feature C, Fig. 4). In both the unmigrated and migrated images (Fig. 4), this thin reflector projects southward to about the hypocenter of the 1987 M 5.9 Whittier Narrows earthquake, a thrust earthquake that occurred on a plane subparallel to reflector C (see balanced cross-section through this hypocenter by Davis and Namson, 1989). Based on these facts, one might speculate that reflector C and the top of the bright reflective zone north of its junction with reflector C is a thrust fault at or near the brittle–ductile boundary. (The brittle–ductile transition may be a zone of concentrated shear.) The 1991 M 5.8 Sierra Madre earthquake, also a thrust earthquake, occurred above the bright reflective zone in a part of the crust characterized by faint north-dipping reflectors that are subparallel to the north-dipping plane of this earthquake (feature H, Fig. 4) These reflectors may represent fault zones that sole into reflective zone DEF (Fig. 4). In contrast, in the northern San Gabriel Mountains, near the San Andreas fault, earthquakes do not extend below about 12-km depth, where another reflective zone (feature G, Fig. 4) appears to extend across the deep projection of the San Andreas fault. Like feature A, feature G changes character across the fault, and probably does not represent a through-going feature.

A preliminary tectonic interpretation of the crust of the San Gabriel Mountains that is consistent with the above observations is given in Fig. 8. We have superposed interpretations of continuous fault zones taken from the unmigrated image (blue lines, Fig. 8) onto a fault interpretation constrained by the migrated image (red lines, Fig. 8), where it is more difficult to draw long, continuous structures. The disruption at the San Andreas fault suggested in the unmigrated image is shown; in the migrated image, one cannot observe such disruption, but disruption is permitted. In the interpretation, two subparallel fault zones, ABC and DEF are drawn. Based on the geometric correlation of zone ABC with earthquakes (see above) and on physical arguments below, this zone may be a young fault. Zone DEF and other reflectors may also be interpreted as young faults, but alternative interpretations as older faults, igneous contacts, or other features, are also possible.

Fig. 6. Super CMP gather for vertical-component (A) and horizontal-component (B) data from region of bright spot. Data have been normalized, converted to envelopes, stacked in offset bins, and 5-s AGC has been applied. Both horizontal components were stacked in (B). Arrows indicate P, S, PP (bright-spot reflection), and PS (converted bright-spot reflection, including both P-to-S and S-to-P conversions). Note absence of critical point for PP, this phase dies at about 20 km. Note that PS is slightly stronger for horizontal components and grows to weak amplitude peak between 10 and 20 km, dying out at greater ranges. (C) Reflection and conversion coefficients for velocity models of San Gabriel Mountains that include bright spot. Note that large amplitudes for PP from positive velocity step predicted at distances of 30–40 km are not seen in data (A), whereas termination of this phase at 20–25 km is consistent with predicted amplitude decrease resulting from negative velocity step. For PS, calculated amplitudes for either negative or positive velocity step are consistent with data (B).

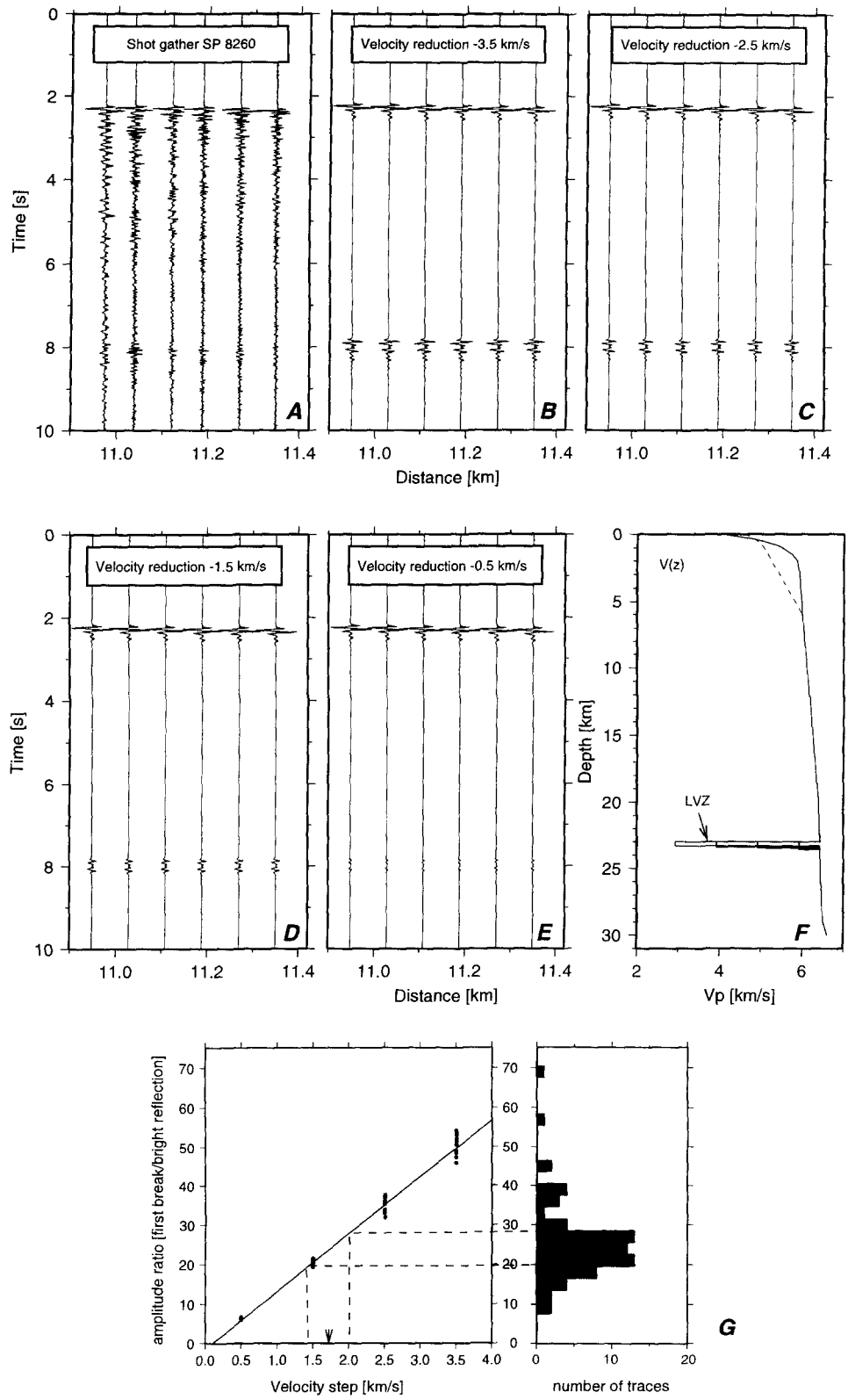
Shot gather SP 8260
Velocity reduction -3.5 km/s
Velocity reduction -2.5 km/s
Velocity reduction -1.5 km/s
Velocity reduction -0.5 km/s
Time [s]
Distance [km]
Depth [km]
V(z)
LVZ
Vp [km/s]
A
B
C
D
E
F
G
amplitude ratio [first break/bright reflection]
Velocity step [km/s]
number of traces

Reflective zones A (the SGMBS) and B abut the lower interpreted fault zone from below. Physical arguments indicate that the rock at the top of zone A is most likely wet crystalline rock with near-lithostatic fluid pressure. Less likely alternatives are that the top of zone A is magma or simply rock of a different composition from rocks above the SGMBS.

If the mid-crust contains fluids, an explanation for the reduced velocities in the SGMBS can be obtained from the results of Nur and Simmons (1969). These researchers document a reduction of more than 1 km/s for both P- and S-wave velocity in low-porosity granite by increasing pore pressure to lithostatic pressure (Nur and Simmons (1969, fig. 3). This mechanism would require a fluid-pressure differential between the rock in the bright zone and the rock above the bright zone, or 'caprock', with lithostatic pressure in the bright zone. Additional reduction of impedance, including reductions of both velocity and density, are possible by opening of macroscopic, fluid-filled fractures (hydrofracture) at lithostatic pressure. Fluid-pressure compartmentalization within the crust and temporal changes of fluid pressure within active fault zones, to values as high as lithostatic, are well-accepted phenomena (e.g., Fyfe et al., 1978; Sibson, 1992, 1994; Hickman et al., 1995; Moore et al., 1995).

Magma may possibly explain the reduced velocities of the SGMBS, but there are no other indicators of magmatic activity in the San Gabriel Mountains. Heat flow is normal in this region (e.g., Lachenbruch and McGarr, 1990), and there is no Holocene volcanism within 100 km of the San Gabriel Mountains.

Finally, a change in composition might possibly also explain the low-velocity zone. Serpentinite and metagraywacke can have velocities less than 5.5 km/s at mid-crustal depths and temperatures (Christensen and Mooney, 1995). There is no evidence of significant serpentinite in the region of the San Gabriel Mountains, although isolated pods are found in the Pelona Schist (Ehlig, 1981). Metagraywacke in the form of the Pelona Schist is present below the Vincent thrust fault (Ehlig, 1981), but samples of this rock analyzed in the laboratory have velocities well above 5.5 km/s at pressures equivalent to the depth of the SGMBS (McCaffree Pellerin and Christensen, 1998).

The interpreted configuration of faults beneath the San Gabriel Mountains includes two major low-angle faults (blue lines, Fig. 8) with splays. The lower one is directly associated with the SGMBS, which may function to cycle fluid at high pressure into the interpreted fault. This fault configuration is not dissimilar to thrust-fault configurations in other fold-and-thrust belts around the earth, such as in the Appalachian Mountains of the eastern United States (e.g., Cook et al., 1983) and the Brooks Range Alaska (e.g., Oldow et al., 1987; Fuis et al., 1997). The deepest interpreted fault could well be the youngest and most recently active, based on analogy with other fold-and-thrust belts. This fault might be termed a 'master' decollement.

6. Conclusion

In conclusion, several factors combine to make the favored interpretation of the SGMBS a young thrust fault zone.

(1) It represents a significant velocity reduction. Such a reduction can be achieved by: (a) a differential change in fluid pressure between the caprock and the bright zone, with lithostatic pressure in the bright zone; (b) presence of a magma; and (c) a change in composition to serpentinite or metagraywacke. The latter two explanations appear unlikely in the San Gabriel Mountains.

(2) It occurs at or near the brittle–ductile transition, as measured by the depth of termination of earthquakes, at least in the southern San Gabriel Mountains.

(3) A thin reflector that diverges upward from the top of this zone projects to the Whittier Narrows

Fig. 7. (A) Observed seismograms from SP 8260 between 10.9- and 11.4-km range. Traces are raw data that have been normalized. (B–E) Synthetic seismograms for same range interval using average 1-D velocity–depth function for San Gabriel Mountains (see F) and low-velocity zones representing velocity reductions of 3.5 (B), 2.5 (C), 1.5 (D), and 0.5 km/s (E). (G) Left-hand side, amplitude ratios (first break/bright-spot reflection) for (B–E) (dots and interpolated solid line). Right-hand side, histogram of amplitude ratios for SP 8260 (distance range 10.5–14.0 km). Comparison of synthetic and observed amplitudes in (G) indicate velocity decrease at bright spot of 1.7 ± 0.3 km/s.

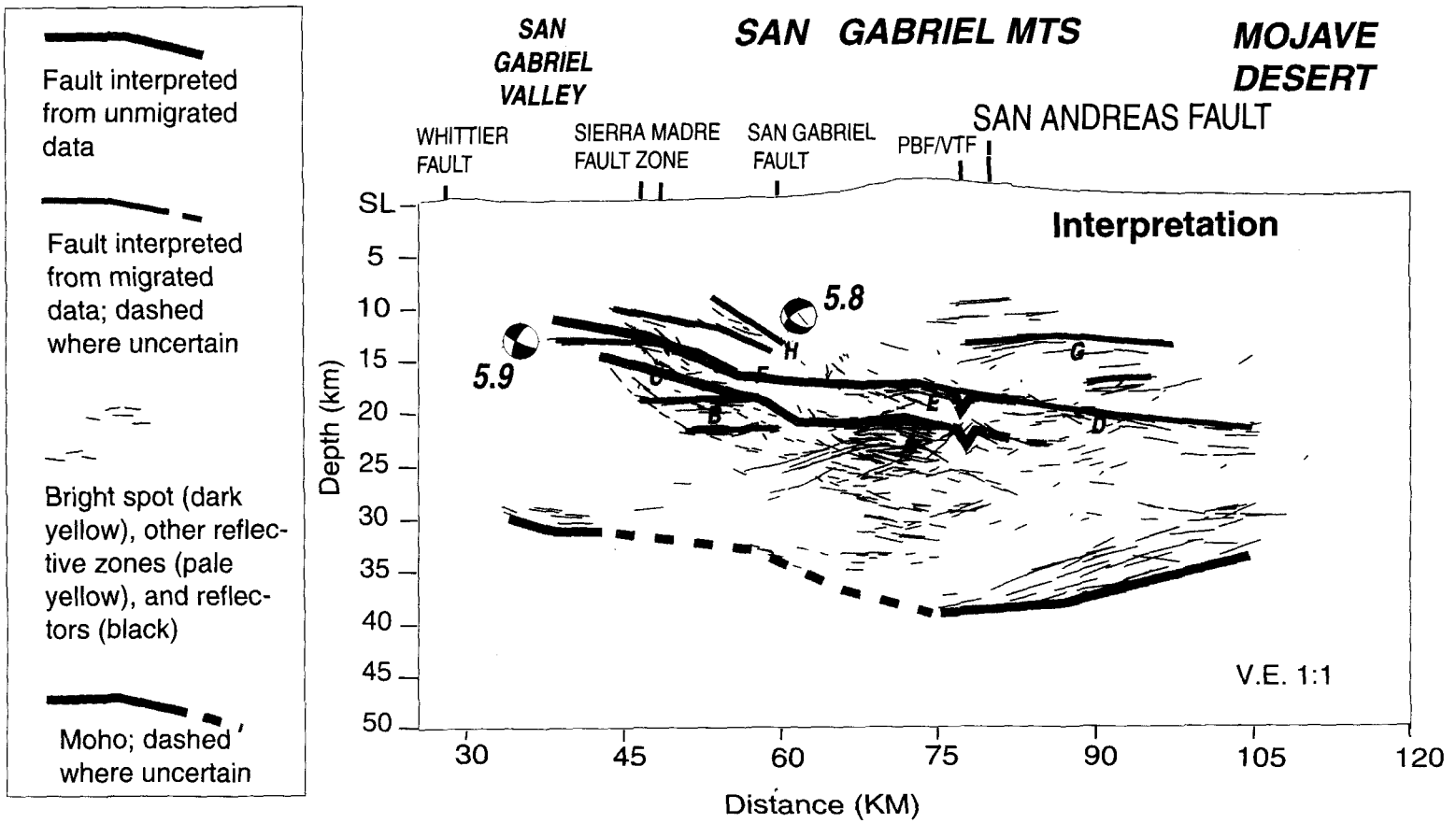

Fig. 8. Preliminary tectonic interpretation of crustal structure of San Gabriel Mountains based on line drawings (Fig. 4). After migration, interpreted faults (red lines) and bright reflective zones (yellow patches) appear less continuous than in unmigrated data (blue lines). Both suggest faults that dip or step up to south toward vicinity of hypocenter of Whittier Narrows earthquake. Bright zones A and B terminate upward at deepest interpreted fault, which may be 'master' decollement. Based on reflections, Moho may reach maximum depth of ~38 km. Letters A–H, reflectors or reflective zones discussed in text.

hypocenter. One could also argue that the bends or disruptions in the reflective zone seen at the San Gabriel and San Andreas faults are actually offsets and that the reflective zone is therefore an older feature, possibly an older fault zone.

Acknowledgements

We thank Simon Klemperer, Dave Lockner, Tom Parsons, Andrew Ross, and an anonymous reviewer for helpful reviews of earlier drafts of this paper. We acknowledge Steve Hickman, Yizhaq Makovsky, Mark Zoback, and Joe Fletcher for helpful discussions. We thank Bill Lutter for supplying an improved velocity inversion (over that in Fuis et al., 1996) for processing the CMP data. We thank Fred Klein and Larry Baker for assistance with the illustrations. We would like to reiterate our thanks to the long list of people acknowledged in Murphy et al. (1996) for their hard work in acquiring the LARSE data, especially Ed Criley, manager of the field operations.

References

Aki, K., Richards, P.G., 1980. Quantitative Seismology, Vol. 1. Freeman, New York, 557 pp.

Aster, R.C., Shearer, P.M., 1991. High-frequency borehole seismograms recorded in the San Jacinto fault zone, southern California, Part 2. Attenuation and site effects. Bull. Seismol. Soc. Am. 81, 1081–1100.

Birch, F., 1961. The velocity of compressional waves in rocks to 10 kilobars, Part 2. J. Geophys. Res. 66, 2199–2224.

Brown, L.D., Chapin, C.E., Sanford, A.R., Kaufman, S., Oliver, J.E., 1980. Deep structure of the Rio Grande Rift from seismic reflection profiling. J. Geophys. Res. 85, 4773–4800.

Christensen, N.I., Mooney, W.D., 1995. Seismic velocity structure and composition of the continental crust: a global view. J. Geophys. Res. 100, 9761–9788.

Cook, F.A., Brown, L.D., Kaufman, S., Oliver, J.A., 1983. The COCORP seismic reflection traverse across the southern Appalachians. Am. Assoc. Pet. Geol. Stud. Geol. 14, 61.

Davis, T., Namson, J., 1989. A cross section of the Los Angeles area: seismically active fold and thrust belt, the 1987 Whittier Narrows earthquake, and earthquake hazard. J. Geophys. Res. 94, 9644–9664.

de Voogd, B., Serpa, L., Brown, L., Hauser, E., Kaufman, S., Oliver, J.E., Troxel, W., Willemin, J., Wright, L.A., 1986. Death Valley bright spot: a midcrustal magma body in the southern Great Basin, California?. Geology 14, 64–67.

Ehlig, P.L., 1981. Origin and tectonic history of the basement terrane of the San Gabriel Mountains, central Transverse Ranges. In: Ernst, W.G. (Ed.), The Geotectonic Development of California. Rubey Vol. 1, Prentice-Hall, Englewood Cliffs, NJ, pp. 253–283.

Fletcher, J.B., Fumal, T., Liu, H.-P., Carroll, L.C., 1990. Near-surface velocities and attenuation at two boreholes near Anza, California, from logging data. Bull. Seismol. Soc. Am. 80, 807–831.

Fuchs, K., Mueller, G., 1971. Computation of synthetic seismograms with the reflectivity method and comparison with observations. Geophys. J. R. Astron. Soc. 23, 417–433.

Fuis, G.S., Okaya, D.A., Clayton, R.W., Lutter, W.J., Ryberg, T., Brocher, T.M., Henyey, T.L., Benthien, M.L., Davis, P.M., Mori, J., Catchings, R.D., ten Brink, U.S., Kohler, M.D., Klitgord, K.D., Bohannon, R.G., 1996. Images of crust beneath southern California will aid study of earthquakes and their effects. EOS Trans. Am. Geophys. Union 77, 173–176.

Fuis, G.S., Murphy, J.M., Lutter, W.J., Moore, T.E., Bird, K.J., 1997. Deep seismic structure and tectonics of northern Alaska: crustal-scale duplexing with deformation extending into the upper mantle. J. Geophys. Res. (Sept. 1997).

Fyfe, W.S., Price, N.J., Thomson, A.B., 1978. Fluids in the Earth's Crust. Elsevier, New York.

Hauksson, E., 1987. Seismotectonics of the Newport–Inglewood fault zone in the Los Angeles basin, southern California. Bull. Seismol. Soc. Am. 77, 539–561.

Hauksson, E., 1994. The 1991 Sierra Madre earthquake sequence in Southern California: seismological and tectonic analysis. Bull. Seismol. Soc. Am. 84, 1058–1074.

Hauksson, E., Jones, L.M., Davis, T.L., Hutton, L.K., Brady, G., Reasenberg, P.A., Michael, A.J., Yerkes, R.F., Williams, P., Reagor, G., Stover, C.W., Bent, A.L., Shakal, A.K., Bufe, C.G., Johnston, M.J.S., Cranswick, E., 1988. The 1987 Whittier Narrows earthquake in the Los Angeles metropolitan area, California. Science 239, 1409–1412.

Hauksson, E., Jones, L.M., Hutton, K., 1995. The 1994 Northridge earthquake sequence in California: seismological and tectonic aspects. J. Geophys. Res. 100, 12335–12355.

Hauser, E., Potter, C., Hauge, T., Burgess, S., Burtch, S., Mutschler, J., Allmendinger, R., Brown, L., Kaufman, S., Oliver, J., 1987. Crustal structure of eastern Nevada from COCORP deep seismic reflection data. Geol. Soc. Am. Bull. 99, 833–844.

Hickman, S., Sibson, R., Bruhn, R., 1995. Introduction to special section: mechanical involvement of fluids in faulting. J. Geophys. Res. 100, 12831–12840.

Hornafius, J.S., Luyendyk, B.P., Terres, R.R., Kamerling, M.J., 1986. Timing and extent of Neogene tectonic rotation in the western Transverse Ranges, California. Geol. Soc. Am. Bull. 97, 1476–1487.

Jarchow, C.M., Thompson, G.A., Catchings, R.D., Mooney, W.D., 1993. Seismic evidence for active magmatic underplating beneath the Basin and Range province, western United States. J. Geophys. Res. 98, 22095–22108.

Kohler, M.D., Davis, P.M., 1997. Crustal thickness variations in southern California from Los Angeles Region Seismic Experiment passive phase teleseismic travel times. Bull. Seismol. Soc. Am., submitted.

Lachenbruch, A.H., McGarr, A., 1990. Stress and heat flow. In: Wallace, R.E. (Ed.), The San Andreas Fault System. U.S. Geol. Surv., Prof. Pap. 1515, 261–277.

Lueschen, E., Wenzel, F., et al., 1987. Near vertical and wide angle seismic surveys in the Black Forest, SW Germany. J. Geophys. 62, 1–30.

Makovsky, Y., Klemperer, S.L., Ratschbacher, L., Brown, L.D., Li, M., Zhao, W., Meng, F., 1996. INDEPTH wide-angle reflection observation of P-wave-to-S-wave conversion from crustal bright spots in Tibet. Science 274, 1690–1691.

McCaffree Pellerin, C.L., Christensen, N.I., 1998. Interpretation of crustal seismic velocities in the San Gabriel–Mojave region, southern California. Tectonophysics 286, 253–271 (this volume).

Moore, J.C., Moore, G.F., Cochrane, G., 1995. Negative-polarity seismic reflections along faults of the Oregon accretionary prism: Indicators of overpressuring. In: Hickman, S., Sibson, R., Bruhn, R. (Eds.), Mechanical Involvement of Fluids in Faulting. J. Geophys. Res. 100, 12895–12906.

Murphy, J.M., Fuis, G.S., Ryberg, T., Okaya, D.A., Criley, E.E., Benthien, M.L., Alvarez, M., Asudeh, I., Kohler, W.M., Glassmoyer, G.N., Robertson, M.C., Bhowmik, J., 1996. Report for explosion data acquired in the 1994 Los Angeles Region Seismic Experiment (LARSE94), Los Angeles, California. U.S. Geol. Surv., Open-File Rep. 96-536, 120.

Nicholson, C., Sorlien, C.C., Atwater, T., Crowell, J.C., Luyendyk, B.P., 1994. Microplate capture, rotation of the western Transverse Ranges, and initiation of the San Andreas transform as a low-angle fault system. Geology 22, 491–495.

Nur, A., Simmons, G., 1969. The effect of saturation on velocity in low porosity rocks. Earth Planet. Sci. Lett. 7, 183–193.

Oldow, J.S., Seidensticker, C.M., Phelps, J.C., Julian, F.E., Gottschalk, R.R., Boler, K.W., Handschy, J.W., Avé Lallemant, H.G., 1987. Balanced cross sections through the central Brooks Range and North Slope, Arctic Alaska. American Association Petroleum Geologists, Tulsa, OK, 19 pp., 8 plates (scales 1 : 500,000 and 1 : 66,666).

Powell, R.E., 1993. Balanced palinspastic reconstruction of prelate Cenozoic paleogeology, southern California: geologic and kinematic constraints on evolution of the San Andreas fault system. Geol. Soc. Am. Mem. 178, 1–106.

Pratt, T.L., Hauser, E.C., Hearn, T.M., Reston, T.J., 1991. Reflection polarity of the midcrustal Surrency bright spot beneath southeastern Georgia: testing the fluid hypothesis. J. Geophys. Res. 96, 10145–10158.

Sanford, A.R., Mott, R.P.Jr., Shuleski, P.J., Rinehart, E.J., Caravella, F.J., Ward, R.M., Wallace, T.C., 1977. Geophysical evidence for a magma body in the crust in the vicinity of Socorro, New Mexico. In: Heacock, J.G. (Ed.), The Earth's Crust: Its Nature and Physical Properties. Am. Geophys. Union, Geophys. Monogr. Ser. 20, 385–403.

Shaw, J.H., Suppe, J., 1996. Earthquake hazards of active blind-thrust faults under the central Los Angeles basin, California. J. Geophys. Res. 101, 8623–8642.

Sibson, R.H., 1992. Implications of fault valve behavior for rupture nucleation and recurrence. Tectonophysics 211, 283–293.

Sibson, R.H., 1994. Crustal stress, faulting, and fluid flow. In: Parnell, J. (Ed.), Geofluids: Origin, Migration, and Evolution of Fluids in Sedimentary Basins. Geol. Soc. London, Spec. Publ. 78, 69–84.

Whitcomb, J.H., 1971. Fault plane solutions of the February 9, 1971, San Fernando earthquake and some aftershocks. U.S. Geol. Surv., Prof. Pap. 733, 30–32.

Wright, T.L., 1991. Structural geology and tectonic evolution of the Los Angeles Basin, California. In: Biddle, K.T. (Ed.), Active Margin Basins. Am. Assoc. Pet. Geol. Mem. 52, 35–134.